PERGAMON

International Journal of Heat and Mass Transfer 46 (2003) 45–53

International Journal of HEAT and MASS TRANSFER

www.elsevier.com/locate/ijhmt

# Molecular dynamics simulation of thermal and thermomechanical phenomena in picosecond laser material interaction

Xinwei Wang [a,*], Xianfan Xu [b]

[a] *Department of Mechanical Engineering, N104 Walter Scott Engineering Center, The University of Nebraska at Lincoln, Lincoln, NE 68588-0656, USA*

[b] *School of Mechanical Engineering, Purdue University, West Lafayette, IN 47907, USA*

Received 2 November 2001; received in revised form 30 June 2002

**Abstract**

In recent years, short pulsed laser materials interaction has attracted considerable attention owing to the rapid development of short pulsed lasers and their potential applications in laser-material processing. In this work, molecular dynamics (MD) simulations are conducted to study the thermal and thermomechanical phenomena induced by picosecond laser heating. The generation and propagation of the stress wave are calculated and depicted in detail. Results of the MD simulation are compared with those obtained with an analytical solution. In addition, a temperature wave as a result of the coupling between temperature and the strain rate is observed, which propagates at the same speed as the stress wave.



## 1. Introduction

Thermal and thermomechanical phenomena in ultrafast laser materials interaction are of great importance for ultrafast laser processing and non-destructive detection. In recent years, a large amount of work has been conducted in this area. Due to the extremely short laser heating duration and the resulting rapid heating and stress development, there are many difficulties to experimentally investigate the thermomechanical waves inside the material. For analytical studies, the continuum approach to solving heat transfer problems and thermal–mechanical coupling can be questionable in these extreme situations. The molecular dynamics (MD) simulation, which solves the movement of atoms or molecules directly, is capable of revealing the mechanism behind the thermal and thermomechanical phenomena in ultrafast laser materials interaction.

In the past several years, many MD simulations of laser materials interaction were reported. Most work was restricted to systems consisting of a small number of atoms. Qualitative results such as the structural change of the target due to laser heating were obtained but few macro-scale phenomena were studied. For instance, Häkkinen and Landman [1] studied the dynamics of phase change in a copper subjected to surface laser heating. Their work provided significant insights pertaining to dynamics, energetics, and structure of surface superheating and melting processes. Other examples include work by Kluge and Ray [2], Chokappa et al. [3], Shibahara and Kotake [4,5], Silvestrelli and Parrinello [6], and Jeschke et al. [7], in which changes of the structure of small systems subjected to ultrafast laser heating were studied. The absorption of laser energy was simulated by exciting the potential energy of atoms [8,9], adding extra energy to the kinetic energy of atoms [10,11], or exciting the vibration of molecules [12–14]. Laser induced thermomechanical waves were studied in a metal [15] by using the Morse potential function [16], in an organic solid using the breathing sphere model [17], and in an argon solid [11].

* Corresponding author. Tel.: +1-402-472-3089; fax: +1-402-472-1465.

*E-mail address:* xinweiw@unlserve.unl.edu (X. Wang).

0017-9310/03/$ - see front matter © 2002 Elsevier Science Ltd. All rights reserved.
PII: S0017-9310(02)00259-4

**Nomenclature**

| | |
|---|---|
| $B$ | bulk modulus |
| $c_p$ | specific heat |
| $F$ | force |
| $G$ | shear modulus |
| $I$ | laser beam intensity |
| $k$ | thermal conductivity |
| $k_B$ | Boltzmann's constant |
| $m$ | mass of an atom |
| $r$ | position of an atom |
| $r_c$ | cutoff distance |
| $r_s$ | the nearest neighbor distance |
| $t$ | time |
| $T$ | temperature |
| $T_0$ | initial temperature |
| $\delta t$ | time step |
| $\Delta T$ | temperature elevation |
| $u$ | displacement |
| $v$ | velocity |

*Greek symbols*

| | |
|---|---|
| $\alpha$ | thermal diffusivity |
| $\beta_T$ | thermal expansion coefficient |
| $\varepsilon$ | LJ well depth parameter |
| $\phi$ | Lennard–Jones potential |
| $\rho$ | density |
| $\sigma$ | stress |
| $\sigma_e$ | equilibrium separation parameter |
| $\tau$ | optical absorption depth |
| $\tau_q$ | thermal relaxation time |

*Subscript*

| | |
|---|---|
| $i$ | index of the atom |

In this work, MD simulations are conducted to study the thermal and thermomechanical phenomena in laser argon interaction using the laser absorption model in which laser energy is added to the kinetic energy of atoms. Various systems are investigated which consist of up to 1,944,000 atoms, which is a suitable number to be handled by the authors' computer resource in terms of suppressing the statistical uncertainty and revealing macro-scale phenomena in laser ablation. This work emphasizes the evolution and propagation of temperature and thermomechanical waves during and after laser heating. For the first time, the thermal–mechanical coupling is studied in detail, which has a strong impact on the temperature distribution and explains the noticeable temperature drop in the near surface region. A temperature wave different from that induced by the non-Fourier effect is observed propagating at the same speed as the stress wave. In Section 2, theories of the MD simulation used in this work are introduced. The simulation results are summarized in Section 3.

## 2. Simulation methods

In this work, an argon crystal at an initial temperature of 50 K illuminated by a picosecond (ps) laser pulse is studied. The basic problem involved is to solve the Newtonian equations for each atom interacting with its neighbors,

$$m_i \frac{\mathrm{d}^2 r_i}{\mathrm{d}t^2} = \sum_{j \neq i} F_{ij} \tag{1}$$

where $m_i$ and $r_i$ stand for the mass and position of atom $i$, respectively. $F_{ij}$ is the interaction force between atoms $i$ and $j$, which is calculated from the Lennard–Jones (LJ) potential as $F_{ij} = -\partial\phi_{ij}/\partial r_{ij}$. The LJ potential $\phi_{ij}$ is written as

$$\phi_{ij} = 4\varepsilon\left[\left(\frac{\sigma_e}{r_{ij}}\right)^{12} - \left(\frac{\sigma_e}{r_{ij}}\right)^{6}\right] \tag{2}$$

where $\varepsilon$ is the LJ well depth parameter, $\sigma_e$ is the equilibrium separation parameter, and $r_{ij} = r_i - r_j$.

In the calculation, the half-step leap-frog scheme—a modification to the velocity Verlet algorithm [18], is employed to solve the movement of atoms. When the distance between particles is larger than a certain distance $r_c$, namely the cutoff distance, the interaction between them is negligible, and no interaction calculation is necessary. The interaction computation of an atom with its neighbors is organized by the cell structure and the linked list methods [18]. In these methods, the computational domain is divided to small cells with a characteristic size of $r_c$, and each atom is sorted into a certain cell based on its position. Only the interaction between atoms in adjacent cells is considered.

The laser beam absorption in the target is simulated by exciting the kinetic energy of atoms, and is fulfilled by scaling the velocities of all atoms in each cell by an appropriate factor. The laser beam is assumed to be absorbed exponentially with an optical absorption depth $\tau$,

$$\frac{\mathrm{d}I}{\mathrm{d}z} = -I(z)/\tau \tag{3}$$

This laser energy absorption model de-emphasizes the details of laser materials interaction, in which the quantum mechanical effect needs to be accounted for. However, the time scale for the process of laser energy absorption (<1 ps) is much smaller than the time scale

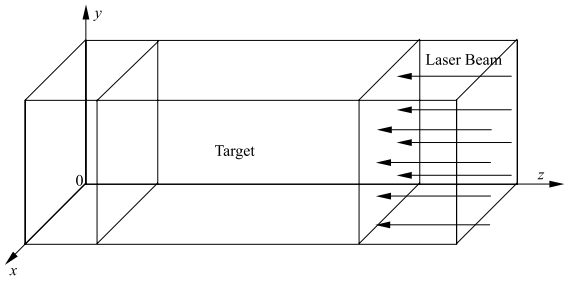


Fig. 1. Schematic of the computational domain for MD simulations.

considered in this work. Therefore, without knowing the details of the laser materials interaction, the thermal and thermomechanical effect can still be investigated using the current absorption model. In this work, $\tau$ is chosen to be 2.5 nm to account for the effect of volumetric absorption of the laser beam. The laser pulse is assumed to have a temporal Gaussian distribution with a full width at half maximum (FWHM) of 5 ps centered at 10 ps.

The schematic of the computational domain is shown in Fig. 1. Extra spaces are added above and below the target, which allow the macro-motion of atoms in the $z$ direction. Periodic boundary conditions are implemented on boundaries in the $x$ and $y$ directions, and free boundary conditions on boundaries in the $z$ direction. The first step of the calculation is to initialize the system to thermal equilibrium before laser heating starts, which is achieved by a thermal equilibrium calculation. In this calculation, the target is initially constructed based on the fcc lattice structure with the (1 0 0) surface facing the laser beam. The nearest neighbor distance, $r_s$, in the fcc lattice of argon depends on temperature $T$, and is calculated using the expression given by Broughton and Gilmer [19],

$$\frac{r_s}{\sigma_e} = 1.0964 + 0.054792\left(\frac{k_B T}{\varepsilon}\right) + 0.014743\left(\frac{k_B T}{\varepsilon}\right)^2 + 0.083484\left(\frac{k_B T}{\varepsilon}\right)^3 - 0.23653\left(\frac{k_B T}{\varepsilon}\right)^4 + 0.25057\left(\frac{k_B T}{\varepsilon}\right)^5 \quad (4)$$

The initial velocities of atoms are specified randomly from a Gaussian distribution based on the specified temperature of 50 K using the following formula

$$\frac{1}{2} m \sum_{i=1}^{3} v_i^2 = \frac{3}{2} k_B T \quad (5)$$

Before laser heating starts, the sample is thermalized for 100 ps to reach thermal equilibrium. The values of the parameters used in the simulation are listed in Table 1.

Table 1
The values of the parameters used in the simulation

| Parameter | Value |
|---|---|
| $\varepsilon$, LJ well depth parameter (J) | $1.653 \times 10^{-21}$ |
| $\sigma_e$, LJ equilibrium separation (Å) | 3.406 |
| $m$, Argon atomic mass (kg) | $66.3 \times 10^{-27}$ |
| $k_B$, Boltzmann's constant (J/K) | $1.38 \times 10^{-23}$ |
| $a$, Lattice constant (Å) | 5.414 |
| $r_c$, Cut off distance (Å) | 8.515 |
| $\tau$, Laser beam absorption depth (nm) | 2.5 |
| $\delta t$, Time step (fs) | 25 |

Table 2
The properties of argon used in the calculation

| Parameter | Value |
|---|---|
| $\rho$, Density (kg/m$^3$) | $1.69 \times 10^3$ |
| $k$, Thermal conductivity (W/m K) | 0.247 |
| $c_p$, Specific heat (J/kg K) | $8.48 \times 10^2$ |
| $G$, Shear modulus (kg/s$^2$ m) | $8.03 \times 10^8$ |
| $B$, Bulk modulus (kg/s$^2$ m) | $2.17 \times 10^9$ |
| $\beta_T$, Volumetric thermal expansion coefficient (1/K) | $1.45 \times 10^{-3}$ |
| $\tau_q$, Thermal relaxation time (s) | $5.13 \times 10^{-13}$ |

The MD simulation results are compared with the analytical solutions to the following equations [20]:

$$\frac{\tau_q}{\alpha}\frac{\partial^2 T}{\partial t^2} + \frac{1}{\alpha}\frac{\partial T}{\partial t} = \frac{\partial^2 T}{\partial z^2} + \frac{1}{k\tau}(I + \tau_q \dot{I})e^{-z/\tau} - \frac{B\beta_T T_0}{k}\left(\frac{\partial^2 u}{\partial z \partial t} + \tau_q \frac{\partial^3 u}{\partial z \partial t^2}\right) \quad (6)$$

$$\rho \frac{\partial^2 u}{\partial t^2} = \left(B + \frac{4}{3}G\right)\frac{\partial^2 u}{\partial z^2} - B\beta_T \frac{\partial T}{\partial z} \quad (7)$$

In the foregoing equations, $\alpha$ is the thermal diffusivity, $k$ is the thermal conductivity, $\rho$ is the density, $B$ and $G$ are the bulk and shear moduli of elasticity, $\beta_T$ is the volumetric thermal expansion coefficient, and $T_0$ is the initial temperature of the target. $\tau_q$ is the thermal relaxation time, which is introduced to account for the non-Fourier effect in ultrafast laser heating [21]. Details of the analytical solutions are described elsewhere [20]. The properties of argon are treated as constants. It is estimated that the average temperature of the argon solid in the near surface region is around 60 K for the fluence of 0.12 J/m$^2$. Therefore, the properties of argon at 60 K are used, and are listed in Table 2 [22,23]. The thermal conductivity and specific heat have been adjusted based on the MD simulation results [24].

## 3. Results and discussions

In this work, the thermal and thermomechanial waves induced by ps laser heating as well as the thermal–mechanical coupling are emphasized. Ablation and the

structural change of the target induced by ps laser heating are published elsewhere [24].

### 3.1. Comparison between the MD simulation and the analytical solution

The thermal and thermomechanical phenomena induced by pulsed laser heating at a laser fluence below the melting threshold are first presented. An argon sample with 90 fcc unit cells in both $x$ and $y$ directions and 60 fcc unit cells in the $z$ direction is illuminated by a pulsed laser with a fluence of 0.12 J/m$^2$. The number of the total atoms under study is 1,944,000. The target measures 48.73 nm in both $x$ and $y$ directions, and 32.48 nm in the $z$ direction.

Fig. 2 compares the temperature distributions obtained from the MD simulation and the analytical solution. It is seen that the results of the MD simulation agree well with those of the analytical solution. At 20 and 25 ps, a thermal wave is observed clearly, which is enlarged in the inset. It needs to be pointed out that this thermal wave is not the one induced by the non-Fourier effect. In the present situation, the non-Fourier effect should have an insignificant effect on heat transfer due to the relatively small thermal relaxation time (~1 ps). The thermal wave shown in Fig. 2 originates from the localized heating due to the coupling between the temperature and the strain rate. From Eq. (6), it can be seen that the local temperature change ($\Delta T$) due to the coupling between the temperature and the strain rate is proportional to the local strain rate, $\rho c_p \partial T/\partial t \sim -B\beta_T T_0 \partial^2 u/(\partial z \partial t)$. Or, the temperature change is related to stress ($\sigma$) as

$$\partial T/\partial t \sim -B/(B + 4/3G)\beta_T T_0/(\rho c_p)\partial\sigma/\partial t \quad (8)$$

Fig. 2 also shows some discrepancy between the results obtained by the MD simulation and the analytical solution. It is seen that in the near surface region, the temperature obtained by the MD simulation is a little higher than that by the analytical solution. In addition, it is evident that the thermal wave obtained by the MD simulation has a larger amplitude and a time delay in comparison with that by the analytical solution. Reasons for these discrepancies will be discussed later.

The evolution of the displacement obtained by the MD simulation and the analytical solution is shown in Fig. 3. It is seen from Fig. 3 that the MD simulation and

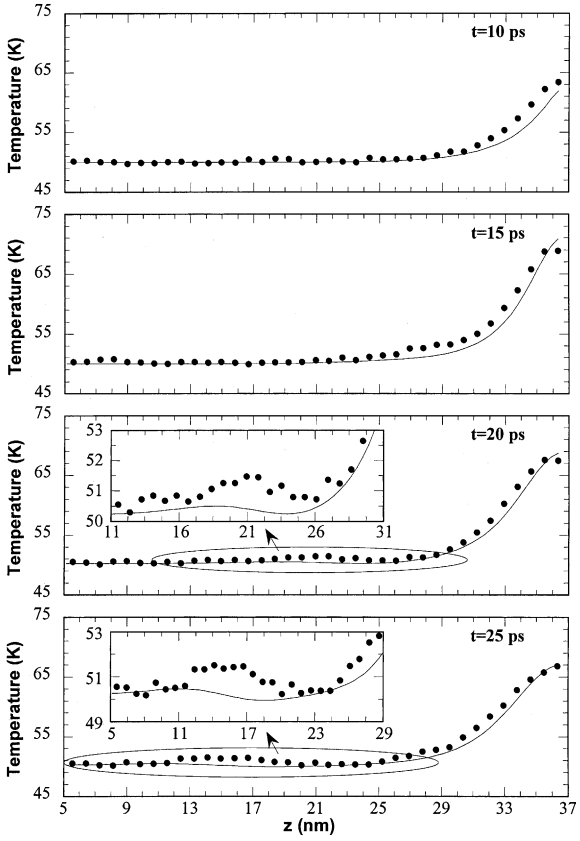


Fig. 2. Temperature distribution in the target. (● ● ●) MD simulation; (—) analytical solution.

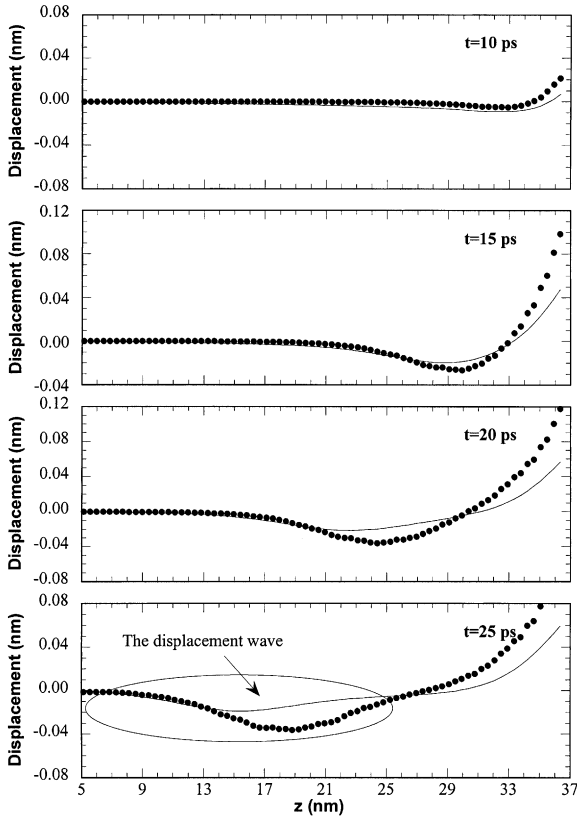


Fig. 3. Evolution of the displacement in the target. (● ● ●) MD simulation; (—) analytical solution.

the analytical solution predict the same trend of displacement. At 25 ps, a displacement wave is formed, which is marked with a circle. The stress induced by laser heating is displayed in Fig. 4. In the MD simulation, the stress on an interested cross-sectional area is calculated by adding all the force between each pair of atoms located on opposite sides of the cross-section, then dividing the total force by the area of the cross-section.

A close look at Figs. 3 and 4 reveals that the displacement and stress predicted by the MD simulation have a larger magnitude compared with those by the analytical solution. Constant properties are used in the analytical solution, which under-predict the displacement and stress as well as the temperature field. In addition, a time delay is observed for the MD simulation results relative to those obtained by the analytical solution. This is because in the MD simulation, the laser energy is directly deposited in the form of kinetic energy, which does not induce a displacement and stress immediately. It takes time for the kinetic energy to be transformed to the potential energy, which in turn results in the displacement and stress. Therefore, the displacement, stress, and the temperature wave induced by the coupling between the temperature and the strain rate predicted by the MD simulation appear behind those by the analytical solution.

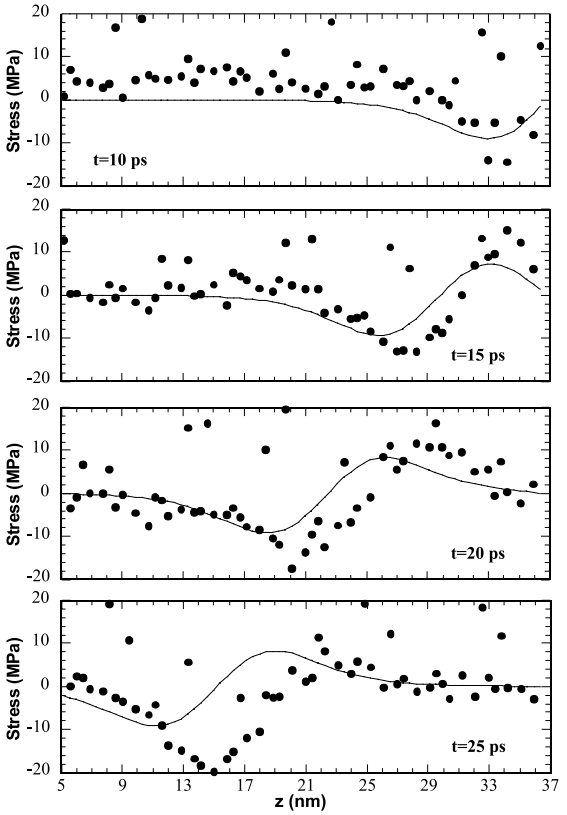


Fig. 4. Stress distribution in the target. (● ● ●) MD simulation; (—) analytical solution.

### 3.2. Thermal and thermomechanical waves accompanying laser ablation

In this study, the target is illuminated by a stronger pulsed laser of a fluence of 0.7 J/m$^2$, which causes ablation. Only the MD simulation is conducted since the analytical solution is not valid for ablation. Fig. 5 shows the temperature distribution in a target with 90 fcc unit cells in both $x$ and $y$ directions, and 15 fcc unit cells in the $z$ direction. An interesting phenomenon is observed in Fig. 5 where a local temperature minimum appears at about 10 nm at 20 and 25 ps, which are marked by arrows. These minimum temperatures are caused by the thermal waves due to the coupling between the temperature and the strain rate. In order to confirm the existence of the thermal wave and to observe its propagation in space, a longer target is studied, which has 32 fcc unit cells in both $x$ and $y$ directions, and 320 fcc unit cells in the $z$ direction. This target consists of 1,310,720 atoms, and measures 17.32 nm in both $x$ and $y$ directions, and 173.25 nm in the $z$ direction. The temperature distribution and the stress at different times are shown in Fig. 6. It is noticed that the minimum temperatures are recaptured at 20 and 25 ps in the near surface region, and are marked with arrows. The minimum temperatures appear at the location where the maximum tensile stress appears. In addition, a local maximum temperature is observed at the location where the maximum compressive stress appears. These temperature–stress pairs again indicate the coupling between the stress and the thermal wave. Eq. (8) demonstrates that the thermal wave and the stress wave have opposite signs, which are confirmed by the results shown in Fig. 6. Using Eq. (8), it is estimated that that the maximum compressive stress

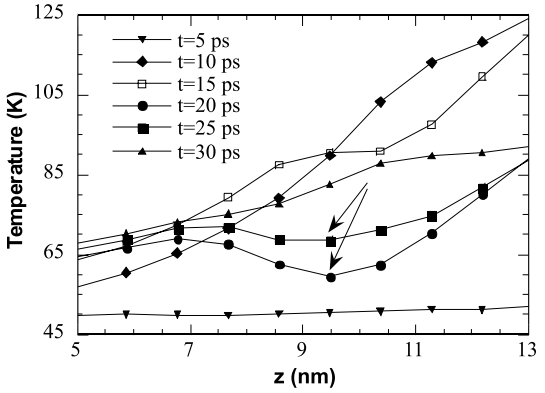


Fig. 5. Temperature distribution in the target.

at 40 ps induces a local temperature elevation of around 2 K. The results of the MD simulation show a temperature elevation of about 3 K indicated in the plot at 40 ps. This discrepancy arises form the inaccuracy of the material properties used in the analytical solution as discussed before.

Fig. 7 shows the development of displacement and stress during laser heating as well as their propagation and reflection on the back side of the target obtained from the MD simulation. The stress shows some statistical noises resulting from the MD simulation. The fitted line shows proper shapes of the stress wave. It is evident

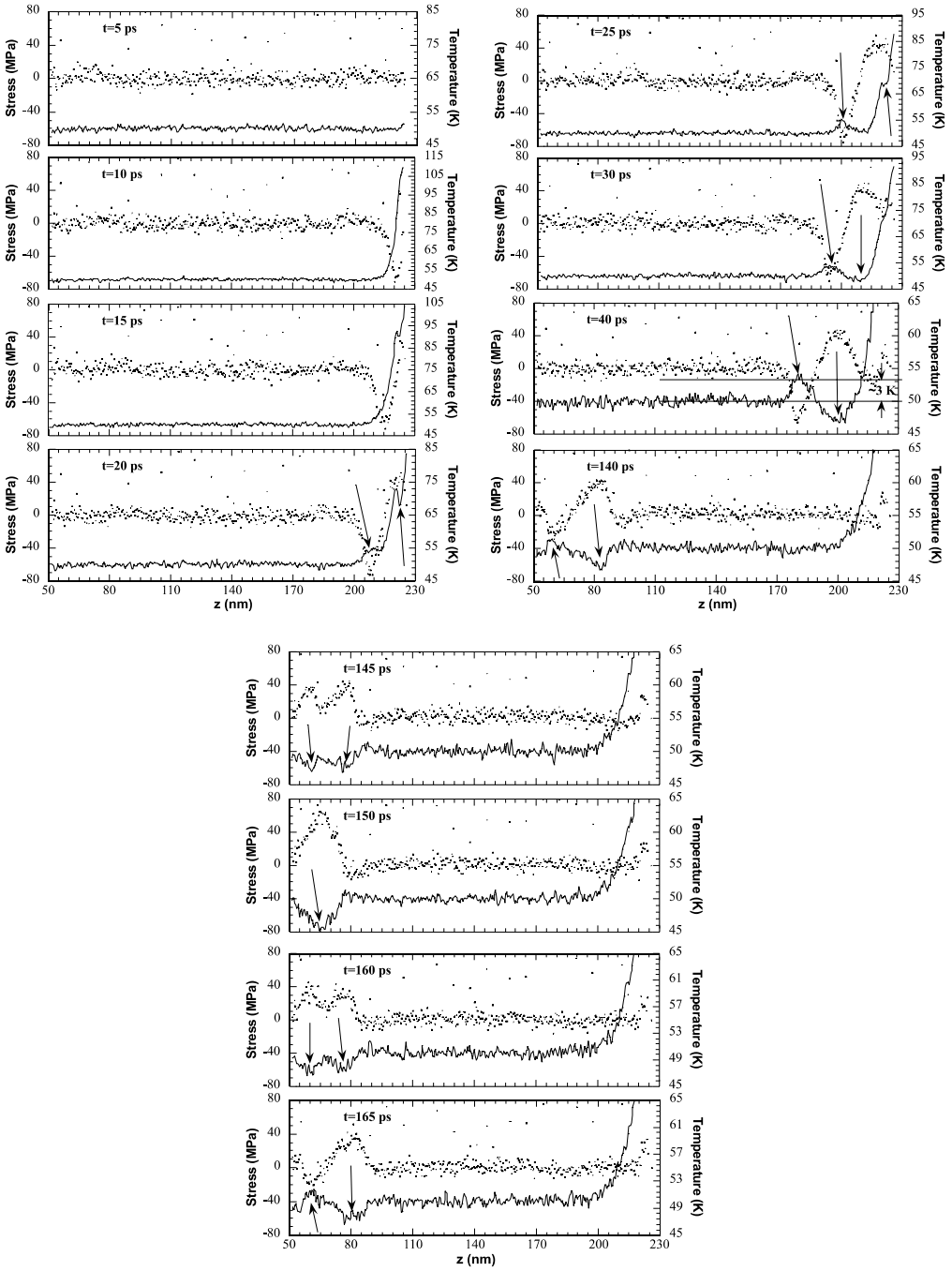


Fig. 6. Temperature and stress distributions in the target. (···) stress; (—) temperature.

in Fig. 7 that at 15 ps, a tensile stress emerges in the near surface region. The displacement at the surface is positive (towards outside) due to thermal expansion, while in the region close to the surface, a negative displacement occurs due to compression (shown in plots at 15 and 20 ps). At 40 ps, the displacement and stress waves are fully developed.

The displacement and stress waves are reflected when they reach the back side of the target. This reflecting process is demonstrated in the plots from 140 to 165 ps.

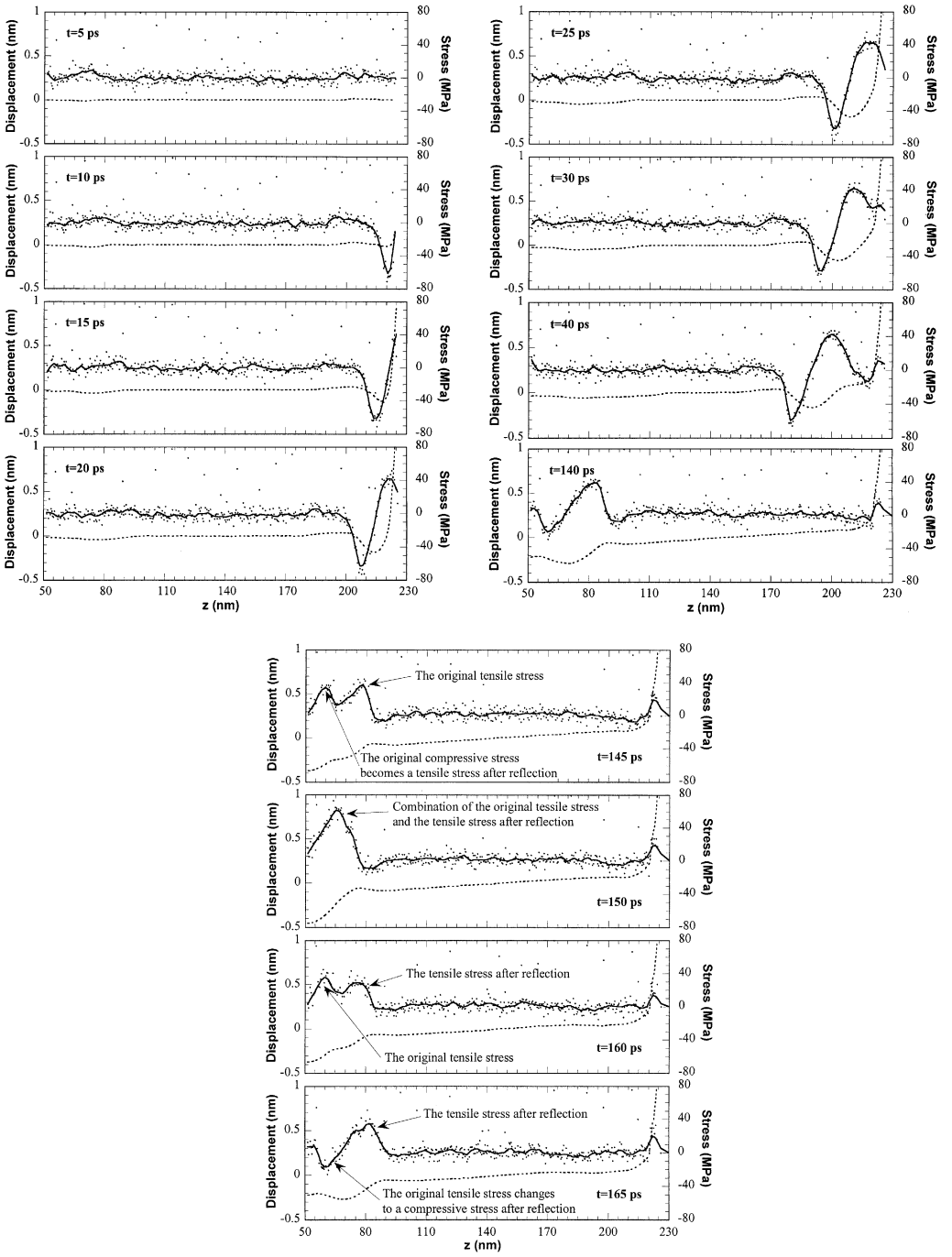


Fig. 7. Development of the displacement and stress in the target. (– – –) displacement; (· · ·) stress; (—) fitted curve of the stress to guide the eye.

At 145 ps, the front of the stress wave, which is compressive, reaches the back side of the target and is reflected. After reflection, the compressive stress becomes tensile. At 150 ps, this tensile stress combines with the tensile stress of the original stress wave, forming a stronger tensile stress wave. At 160 ps, the tensile stress from reflection and the tensile stress of the original stress wave separate. The tensile stress of the original stress is reflected and becomes compressive, which is shown in the plot at 165 ps. The original stress wave is completely reversed after reflection. Based on the locations of the peak compressive stress at different times, the speed of the stress wave along the [1 0 0] direction is calculated to be 1333 m/s. This value agrees well with the experimental sound speed (1425 m/s) of argon in the [1 0 0] direction [22].

## 4. Conclusion

In this work, MD simulations were performed to study the thermal and thermomechanical waves in ps laser interaction with solid argon. The MD simulation results were compared with the results of the analytical solution at a laser fluence below the melting threshold. It was concluded that without phase change, the temperature field predicted by the MD simulation agreed with that by the analytical solution. Discrepancy between the MD simulation and the analytical solutions is caused by the constant properties used in the analytical solution. Temperature waves were observed and successfully explained by the coupling between the temperature and the strain rate. It was also demonstrated that the MD simulation is capable of capturing the details of the development, propagation, and reflection of stress and displacement waves during and after laser heating.

## Acknowledgements

Support for this work by the National Science Foundation (CTS-9624890) is gratefully acknowledged. X. Wang is also grateful for the financial support of the start-up fund from the College of Engineering and Technology and the Department of Mechanical Engineering at the University of Nebraska at Lincoln.

## References

[1] H. Häkkinen, U. Landman, Superheating, melting, and annealing of copper surfaces, Phys. Rev. Lett. 71 (1993) 1023–1026.
[2] M.D. Kluge, J.R. Ray, Pulsed laser melting of silicon: A molecular dynamics study, J. Chem. Phys. 87 (1987) 2336–2339.
[3] D.K. Chokappa, S.J. Cook, P. Clancy, Nonequilibrium simulation method for the study of directed thermal processing, Phys. Rev. B 39 (1989) 10075–10087.
[4] M. Shibahara, S. Kotake, Quantum molecular dynamics study on light-to-heat absorption mechanism: Two metallic atom system, Int. J. Heat Mass Transfer 40 (1997) 3209–3222.
[5] M. Shibahara, S. Kotake, Quantum molecular dynamics study of light-to-heat absorption mechanism in atomic systems, Int. J. Heat Mass Transfer 41 (1998) 839–849.
[6] P.L. Silvestrelli, M. Parrinello, Ab initio molecular dynamics simulation of laser melting of graphite, J. Appl. Phys. 83 (1998) 2478–2483.
[7] H.O. Jeschke, M.E. Garcia, K.H. Bennemann, Theory for laser-induced ultrafast phase transitions in carbon, Appl. Phys. A 69 (1999) S49–S53.
[8] S. Kotake, M. Kuroki, Molecular dynamics study of solid melting and vaporization by laser irradiation, Int. J. Heat Mass Transfer 36 (1993) 2061–2067.
[9] R.F.W. Herrmann, J. Gerlach, E.E.B. Campbell, Ultrashort pulse laser ablation of silicon: An MD simulation study, Appl. Phys. A 66 (1998) 35–42.
[10] E. Ohmura, I. Fukumoto, I. Miyamoto, Modified molecular dynamics simulation on ultrafast laser ablation of metal, in: The International Congress on Applications of Lasers and Electro-Optics, Laser Institute of America, Orlando, 1999, pp. 219–228.
[11] J.I. Etcheverry, M. Mesaros, Molecular dynamics simulation of the production of acoustic waves by pulsed laser irradiation, Phys. Rev. B 60 (1999) 9430–9434.
[12] L.V. Zhigilei, P.B.S. Kodali, B.J. Garrison, Molecular dynamics model for laser ablation and desorption of organic solids, J. Phys. Chem. B 101 (1997) 2028–2037.
[13] L.V. Zhigilei, B.J. Garrison, Computer simulation study of damage and ablation of submicron particles from short-pulse laser irradiation, Appl. Surf. Sci. 127–129 (1998) 142–150.
[14] L.V. Zhigilei, P.B.S. Kodali, B.J. Garrison, A microscopic view of laser ablation, J. Phys. Chem. B 102 (1998) 2845–2853.
[15] E. Ohmura, I. Fukumoto, Molecular dynamics simulation on laser ablation of FCC metal, Int. J. Jpn Soc. Precision Eng. 30 (1996) 128–133.
[16] L.A. Girifalco, V.G. Weizer, Application of the morse potential function to cubic metals, Phys. Rev. 114 (1959) 687–690.
[17] L.V. Zhigilei, B.J. Garrison, Pressure waves in microscopic simulations of laser ablation, Mater. Res. Soc. Symp. Proc. 538 (1999) 491–496.
[18] M.P. Allen, D.J. Tildesley, Computer Simulation of Liquids, Clarendon Press, Oxford, 1987 (Chapter 3 and 5).
[19] J.Q. Broughton, G.H. Gilmer, Molecular dynamics investigation of the crystal–fluid interface. I. Bulk properties, J. Chem. Phys. 79 (1983) 5095–5104.
[20] X. Wang, X. Xu, Thermoelastic wave induced by pulsed laser heating, Appl. Phys. A 73 (2001) 107–144.
[21] D.Y. Tzou, Macro- to Microscale Heat Transfer—The Lagging Behavior, Taylor and Francis, Washington, 1996.
[22] G.J. Keeler, D.N. Batchelder, Measurement of the elastic constants of argon from 3 to 77 K, J. Phys. C: Solid State Phys. 3 (1970) 510–522.

[23] O.G. Peterson, D.N. Batchelder, R.O. Simmons, Measurements of X-ray lattice constant, thermal expansivity, and isothermal compressibility of argon crystals, Phys. Rev. 150 (1996) 703–711.

[24] X. Wang, X. Xu, Molecular Dynamics Simulation of Heat Transfer and Phase Change during Laser Material Interaction, Proceedings of the 35th National Heat Transfer Conference, ASME, 2001, paper# NHTC 2001-20070.